3-D Structure of Nanosized Catalysts by High-Energy X-ray Diffraction and Reverse Monte Carlo Simulations: Study of Ru

N. Bedford,[†] C. Dablemont,[‡] G. Viau,[‡] P. Chupas,[§] and V. Petkov*,[†]

Department of Physics, Central Michigan University, Mt. Pleasant, Michigan 48859, ITODYS, University Paris 7-Denis Diderot, UMR 7086, F 75251, Paris Cedex 05, France, and Advanced Photon Source, Argonne National Laboratory, Argonne, Illinois 60439

Received: July 4, 2007; In Final Form: September 20, 2007

Ruthenium exhibits a high catalytic activity that is further enhanced when the material is used as nanosized particles. The origin of the enhanced performance lies in the highly increased surface to volume ratio and, often, to the surface/environment-driven structural relaxation taking place at the nanoscale. In this paper, we show how high-energy X-ray diffraction, atomic pair distribution function analysis, and reverse Monte Carlo simulations may be used to determine the 3-D structure of nanoparticle catalysts such as Ru with sizes less than 5 nm. Ruthenium particles that are 4 nm in size are found to possess a hexagonal close packed-type structure, similar to that found in bulk Ru. Particles that are only 2 nm in size are heavily disordered and consist of a Ru core and a Ru−S skin due to the usage of thiol-based capping agents. This work is the first application of an approach for determining the atomic-scale structure of nanosized catalysts based entirely on experimental diffraction data. The new structural information is a starting point for a better understanding of the structure−property relationship and, hence, for the design of improved nanosized catalysts, including Ru.

Introduction

Catalysis is a broad research and industry field, and its great economic value is not the catalysts per se but the reaction chemistry they facilitate and/or enable. For many years, research has been directed toward the discovery of new catalysts with improved efficiency and selectivity. Recently, interest has shifted to nanosized catalysts since they show an improved activity due to the greatly increased surface to volume ratio. A large number of atoms from a nanosized catalyst (e.g., almost any second atom from a spherical particle of size 2−3 nm) is, however, located very close or directly at its surface, and thus directly exposed to the catalyst's environment. Surface- and/or environment- and/or small size-driven structural relaxation is to be expected, and often atoms in nanosized (less than 5 nm) catalytic particles end up arranged in a 3-D structure that is different from the one they adopt in their bulk counterparts (i.e., nanosized catalysts often do not appear as a nanosized piece of the corresponding bulk material).[1,2] This may have a profound effect on their structure−sensitive properties, including the catalytic ones. Clearly, any further progress in the field depends critically on the ability to assess the 3-D structure of nanosized catalysts in very good detail.

Traditionally, the 3-D structure of materials has been determined by Bragg X-ray diffraction (XRD). Bragg XRD is, however, not very informative in the case of nanosized materials because they act as a diffraction grating of a very limited length of structural coherence and, hence, produce diffraction patterns with a few, if any, Bragg-like peaks. This has pressed scientists to employ other structure sensitive techniques such as XANES, EXAFS, AFM, and TEM. Spectroscopy techniques such as XANES and EXAFS provide important information about the valence state and nearest-atomic neighbor arrangement but are not sensitive to the longer range atomic structure in materials. Thus, for example, EXAFS would hardly discriminate between a face centered cubic (fcc) and a hexagonal close packed (hcp) structure both occurring with metallic (zero valence state) nanoparticles and exhibiting the same number of 12 first atomic neighbors. On the other hand, techniques such as TEM and AFM are indispensable in revealing the nanoparticle morphology (i.e., size and shape), but what they provide is indeed an image that is a projection down an axis. Hence, in general, imaging techniques are not very sensitive to the 3-D atomic ordering inside nanosized particles either. Recently, it has been demonstrated that a nontraditional approach involving high-energy XRD and atomic pair distribution function (PDF) analysis may be employed to determine the 3-D atomic ordering in nanosized materials[3−7] with success. Here, we apply it to Ru particles with a size less than 5 nm. Bulk ruthenium and Ru-based alloys are among the most widely used catalysts. Nanosized Ru performs even better in important applications such as carbon nanotube growth,[8] selective reduction of NO,[9] and biomass refining.[10] We find that ruthenium particles with a mean size of 4 nm exhibit a hcp-type structure, similar to that found in bulk Ru. Ruthenium particles with a mean size of 2 nm are much more disordered and may only be described by a nonperiodic atomic configuration. The configuration is constructed by reverse Monte Carlo simulations based on experimental PDF data.

Experimental Procedures

Sample Preparation. Several methods for the preparation of nanosized Ru particles have been developed differing in the chemicals and stabilizing agents used to grow and prevent the agglomeration, respectively, of the primary particles.[10−17] Monodisperse Ru particles with a mean size of approximately 4 and 2 nm, and with different capping agents, were synthesized

* Corresponding author. E-mail: petkov@phy.cmich.edu.
[†] Central Michigan University.
[‡] University Paris 7-Denis Diderot.
[§] Argonne National Laboratory.

10.1021/jp0752062 CCC: $37.00
Published on Web 11/16/2007

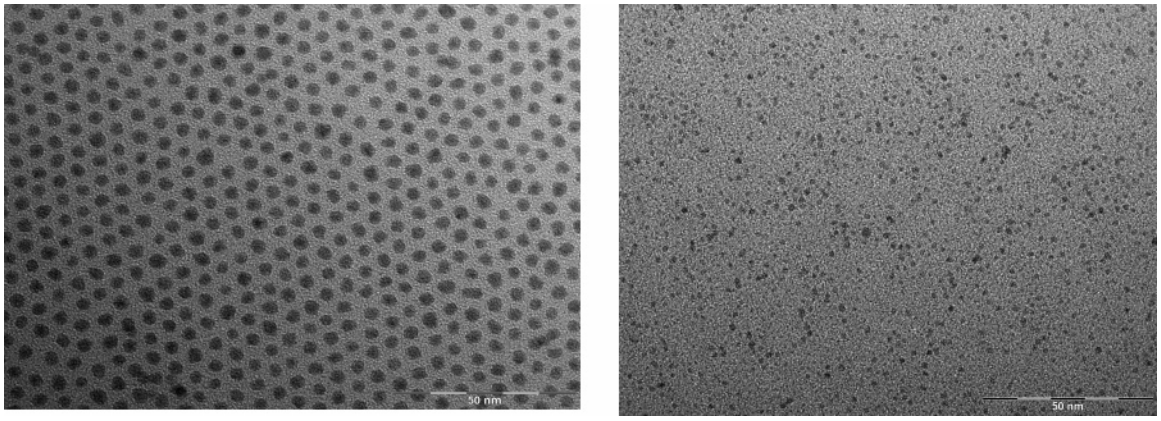

Figure 1. TEM images of thiol-capped 4 nm (left) and 2 nm (right) Ru particles.

as follows: ruthenium acetate/polyol particles of a size of 4 nm were obtained by the reduction of ruthenium trichloride in a hot solution of sodium acetate in 1,2-propanediol. The solution was heated with an acetate concentration of 1.0×10^{-2} M at 150 °C for 15 min under stirring. Resulting nanosized particles were removed from the solution by centrifugation, washed with ethanol, and dried in air. Thiol-capped Ru particles of a mean size of 4 and 2 nm were prepared essentially by the same procedure. Their size was adjusted by varying the acetate concentration and the reaction temperature. The particles were further coated by dodecanethiol at room temperature. This was done by stirring a solution of dodecanethiol in toluene with the primary suspension of Ru particles obtained in polyol. The 4 nm thiol-coated particles were precipitated by the addition of ethanol and recovered by centrifugation, washed with ethanol, and then dried in air at 50 °C. The solution containing 2 nm thiol-coated particles was evaporated to dryness, and the solid particles were washed with ethanol and then again dried in air at 50 °C. The presence of S atoms in the thiol-capped nanoparticles was confirmed by EDX spectroscopy. It was found that the S/Ru ratio was always higher for the 2 nm than the 4 nm particles. The as-obtained particles were characterized by transmission electron microscopy (TEM). Representative TEM images are shown in Figure 1. As can be seen, both 4 and 2 nm ruthenium particles appear to be rounded in shape. The actual mean diameter was found to be 3.8 and 1.7 nm, respectively, for the particles called 4 and 2 nm throughout the text. The particle size distribution is very narrow for the 4 nm size particles with $\sigma/d_m = 10\%$. It is much broader for the 2 nm particles, with σ reaching 20% of the mean particle diameter. Here, σ and d_m are the standard deviation and mean particle diameter, respectively, estimated by an image analysis of ca. 250 particles.

X-ray Diffraction Measurements. High-energy XRD experiments were carried out at the 11-ID−-B beamline (Advanced Photon Source, Argonne National Laboratory) using a synchrotron radiation of energy of 90.48 keV ($\lambda = 0.1372$ Å) at room temperature. Dry nanopaticles, acetate/polyol-based with a mean size of 4 nm as well as acetate/polyol-based and further thiol-capped with a mean size of 4 and 2 nm, were sandwiched between Kapton foils and measured in transmission geometry. Bulk Ru (from Alfa Aesar; 99.9% purity; crystallite grain size of ~1000 nm) was also measured and used as a reference material. The scattered radiation was collected with a large area (General Electric) detector. Experimental XRD patterns are shown in Figure 2. Thanks to the high-energy/short wavelength of synchrotron radiation X-rays used, XRD data were collected over quite a wide region (0−30 Å^{-1}) of reciprocal space vectors, Q. Here, $Q = 4\pi (\sin \theta)/\lambda$, where θ is half the angle between the incoming and the outgoing X-rays and λ is the wavelength of the radiation used. Besides, the higher flux of synchrotron radiation X-rays and the usage of a large area detector yielded XRD data of a very good statistical accuracy. Both an extended Q-range and a high statistical accuracy are a prerequisite to the success of the atomic pair distribution function (PDF) data analysis employed here.[3,19]

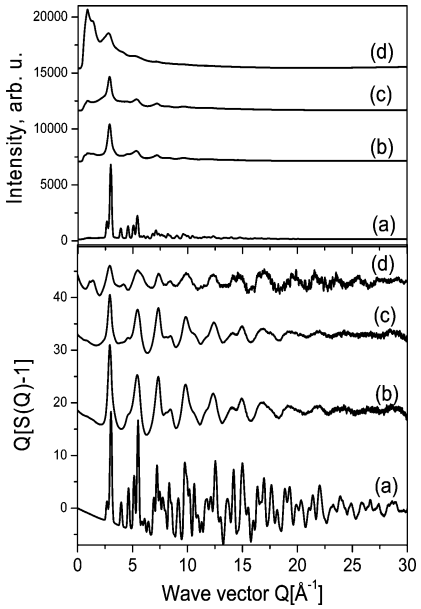

Figure 2. Synchrotron XRD patterns (upper) and corresponding reduced structure factors (lower) for crystalline Ru (a), 4 nm Ru/acetate (b), 4 nm Ru/thiol (c), and 2 nm Ru/thiol (d) particles.

Results

As can be seen in Figure 2, the XRD pattern of bulk Ru exhibits well-defined Bragg peaks, as can be expected for a long-range ordered material. Such a pattern may be analyzed in a traditional (e.g., Rietveld) way. The analysis has shown that atoms in crystalline ruthenium form a hcp-type structure. This structure may be well-described in terms of a periodic lattice (space group *P*63/*mmc*) with a two atom unit cell of parameters $a = 2.706$ Å and $c = 4.282$ Å.[20] The diffraction patterns of Ru nanosized particles are very diffuse in nature and are impossible to be analyzed in the traditional way. That is why the experimental XRD patterns were considered in terms of the corresponding total reduced structure factor $F(Q) = Q[S(Q) - 1]$ and its Fourier transform—the atomic PDF $G(r) = 4\pi r[\rho(r) - \rho_0]$. Here, $\rho(r)$ and ρ_0 are the local and average atomic number

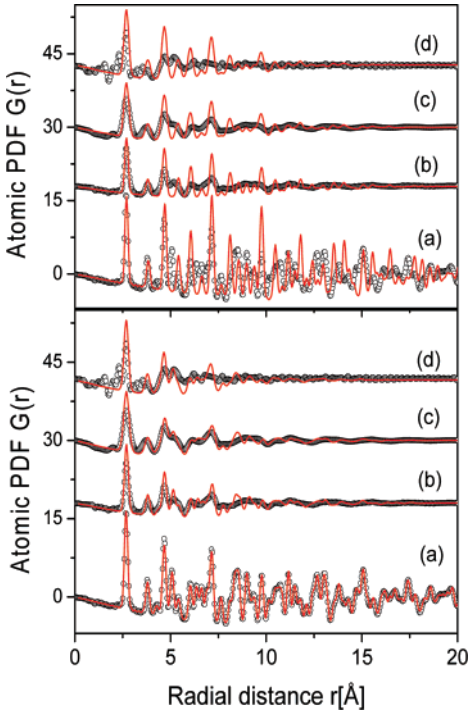

Figure 3. Experimental atomic PDFs (symbols) for crystalline Ru (a), 4 nm Ru/acetate (b), 4 nm Ru/thiol (c), and 2 nm Ru/thiol (d) particles. Model PDFs (solid line in red) based on the fcc (upper part) and hcp (lower part) structures are shown as well.

densities, respectively, and r is the radial distance. The structure factor $S(Q)$ is related to the coherent part, $I^{coh}(Q)$, of the diffraction data as follows:

$$S(Q) = 1 + \left[I^{coh}(Q) - \sum c_i |f_i(Q)|^2\right] / \sum |c_i f_i(Q)|^2 \quad (1)$$

where c_i and f_i are the atomic concentration and X-ray scattering factor, respectively, for the atomic species of type i.[3,19] The reduced structure factors for all ruthenium samples studied are shown in Figure 2 (lower part). The corresponding atomic PDFs $G(r)$ are shown in Figure 3. The processing of XRD data and derivation of $F(Q)/G(r)$ values was performed with the help of the program RAD.[21] An inspection of the data presented in Figure 2 exemplifies the different way the same diffraction features appear and, hence, are accounted for in traditional and high-energy XRD/PDF studies. Traditional XRD patterns are dominated by strong diffraction features at low wave vectors and, hence, are mostly sensitive to the longer range atomic ordering in materials. All diffraction features within a wide range of wave vectors, including higher order ones, appear equally strong in the $F(Q)$ values derived from the traditional XRD patterns. This increases the sensitivity to local (shorter range) atomic ordering, rendering the Fourier couple $F(Q)/G(r)$ a quantity very well-suited to study materials of limited, including nanosized, structural coherence. That Ru particles are such a material is clearly seen in Figure 3, showing their PDFs decaying to zero already at approximately 1 nm. In contrast, the PDF for bulk/polycrystalline Ru persists to much longer interatomic distances. The latter is very well-reproduced by a model based on the well-known hcp structure of crystalline Ru (see Figure 3, lower panel), testifying to the fact that atomic PDFs accurately reflect the 3-D structure of materials. The model PDF was calculated with the help of the program PDFFIT[22] using literature data for the structure of crystalline Ru.[20] Regardless of their very fast decay, the experimental PDFs for Ru nanoparticles show many sharp features and allow an unambiguous structure search and refinement as well. In particular, the experimental PDFs for 4 nm Ru nanoparticles, both treated and untreated with dodecanethiol, are reasonably well-approximated by a model based on a hcp-type structure (shown in Figure 4, right upper panel). A model based on a fcc-type structure (shown in Figure 4, left upper panel) is incompatible with the experimental data as the results presented in Figure 3 show. These model PDFs were calculated with the help of the program PDFFIT as well.[22] The limited length of structural coherence in the 4 nm particles was taken into account as suggested in ref 23 and implemented in refs 11 and 24. Clearly, the extra processing and introducing of a thiol-capping layer does not affect substantially the atomic ordering in 4 nm Ru particles; it is of a hcp-type in both sets of 4 nm particles studied. That atomic ordering, however, is not very perfect since the length of structural coherence (measured by the real space distance, ~1 nm, where the experimental PDFs approach zero) is much shorter than the average nanoparticle size (~4 nm) revealed by TEM. The reduced length of structural coherence indicates the presence of considerable local structural distortions and/or strain in both sets of the 4 nm Ru particles we studied.

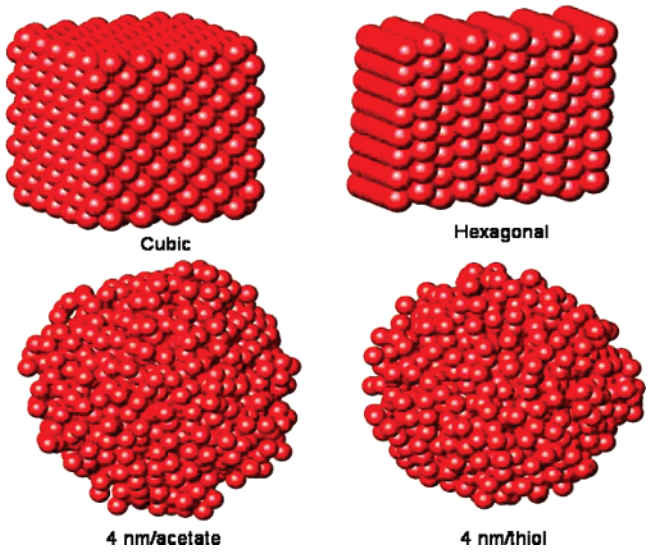

Figure 4. Fragments from the cubic (fcc) and hexagonal (hcp) close packing of atoms occurring in bulk metals (upper). RMC generated models of 4 nm particles (lower).

Neither the fcc- nor the hcp-type structure types reproduced well the experimental PDF data for 2 nm Ru particles (see Figure 3). Besides, the first peak in the experimental PDF for 2 nm particles is split into two components: a high-r one positioned at approximately 2.7 Å and a low-r one− at 2.3 Å (see Figure 4). The high-r one reflects the first neighbor Ru−Ru atomic pairs in metallic Ru (zero valence state). The PDFs for all other Ru samples studied also peak at that distance. The low-r component appears at a bond distance typical for Ru−S atomic pairs, indicating that a considerable fraction of Ru atoms in 2 nm particles is bonded to S atoms likely coming from thiol molecules used as capping agents. Thiol-capped Ru particles with a mean size of 4 nm, however, do not seem to exhibit a considerable number of Ru−S bonds since the corresponding PDF data do not peak at the Ru−S bond distance. The distribution of first atomic neighbor distances in thiol-capped 4 nm Ru particles is, however, considerably broadened when compared to that in 4 nm Ru particles that do not contain sulfur (see Figure 4). The result shows that the usage of thiol-capping agents does not always result in the formation of a substantial (i.e., detectable within the limits of experimental accuracy)

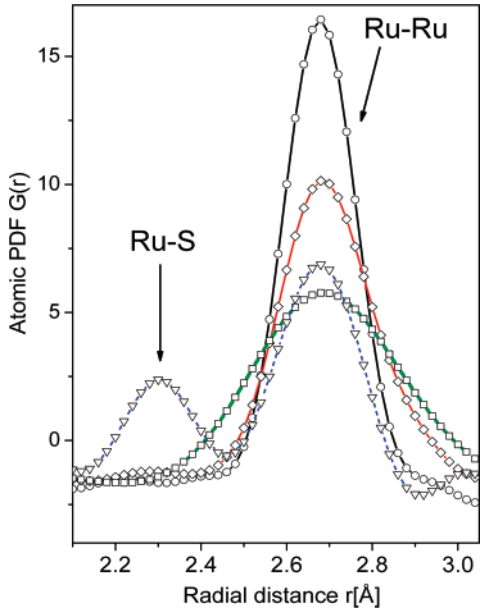

Figure 5. First peak in the experimental atomic PDFs for crystalline Ru (circles), 4 nm Ru/acetate (rhombs), 4 nm Ru/thiol (squares), and 2 nm Ru/thiol (triangles) particles. Solid lines (in color) are a guide to the eye. Peak components are labeled with the corresponding atomic pairs (Ru−S and Ru−Ru).

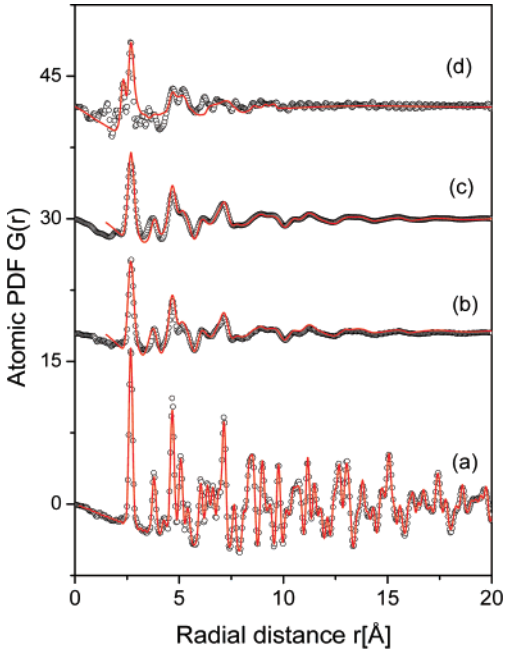

Figure 6. Experimental atomic PDFs (symbols) for crystalline Ru (a), 4 nm Ru/acetate (b), 4 nm Ru/thiol (c), and 2 nm Ru/thiol (d) particles. Model PDFs (solid line in red) based on a periodic (hexagonal-type lattice) (a) and discrete (RMC generated clusters) structures (b−d) are shown as well.

number of sulfur-containing bonds at the nanoparticle surface as is the case with thiol-capped 2 nm particles. This may introduce measurable local structural distortions inside nanoparticles instead, similar to the case of 4 nm thiol-capped particles.

Discussion

The first-round analysis of experimental PDF data clearly showed that a detailed description of the atomic ordering in 4 nm and especially of that in 2 nm Ru nanoparticles requires us to go beyond traditional/perfect lattice-type models. To build structural models that incorporate the presence of a great deal of structural disorder, we employed the reverse Monte Carlo (RMC) modeling technique.[25−27] It does not require prior knowledge of interatomic forces and/or potentials but relies entirely on available experimental information. This is a great advantage since interatomic interactions are not precisely known or not known at all in many cases of practical interest. The RMC technique involves the placing of atoms in a simulation box and moving them around so that the difference between the model computed and the experimental structure-sensitive quantities, the experimental PDF data in our case, becomes as small as possible. We started with the construction of a RMC model for polycrystalline Ru to obtain a set of reference structural parameters, a distribution of bond angles in particular, that reflect the presence of usual thermal disorder (all XRD data were taken at room temperature) in all samples studied. The model consisted of 5760 ruthenium atoms in a box with an edge of length 42 Å. The long-range structural coherence in bulk ruthenium was simulated by imposing periodic boundary conditions. Also, each atom from the model atomic configuration was constrained to have 12 first neighbors as in hcp bulk Ru. A minimum distance of closest approach between two neighboring ruthenium atoms was set to be 2.6 Å. The calculations were performed with the help of the program RMC++.[28] As may be expected, the model converged quickly, reproducing the experimental PDF data very well as can be seen in Figure 6. The distribution of bond angles in the model is shown in Figure 7. The angles seen are close to

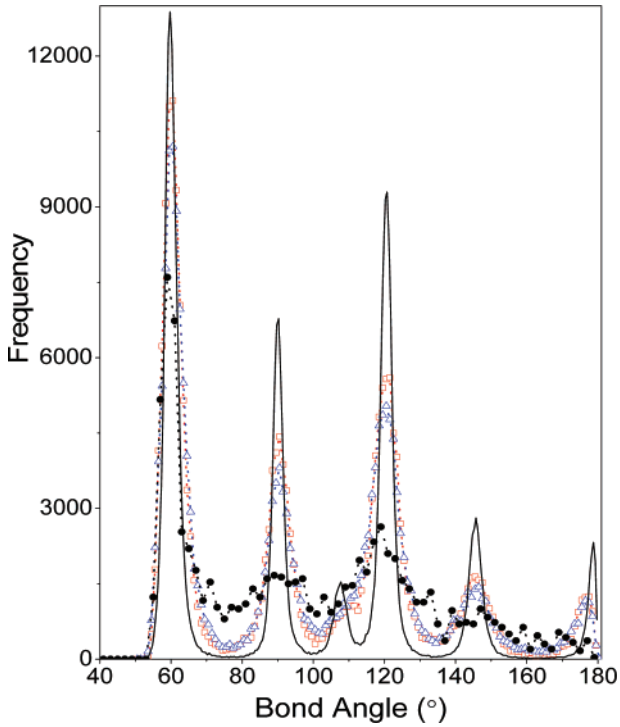

Figure 7. Distribution of bond angles in bulk Ru (solid line) and 4 nm Ru/acetate (squares in red), 4 nm Ru/thiol (triangles in blue), and 2 nm Ru/thiol (full circles) particles.

60, 90, 109.47, 120, 146.44, and 180° that are a fingerprint of the hcp-type (ideal) structure. For reference, the bond angles in the fcc-type (ideal) structure are 60, 90, 120, and 180°. Models for 4 nm particles consisted of 1200 ruthenium atoms in a simulation box with an edge of length 32 Å. Atoms were removed from the vertices of the simulation box to make the model configurations rounded in shape, similar to the 4 nm Ru particles we studied (see the TEM images in Figure 1). The calculations were performed keeping an ample empty space

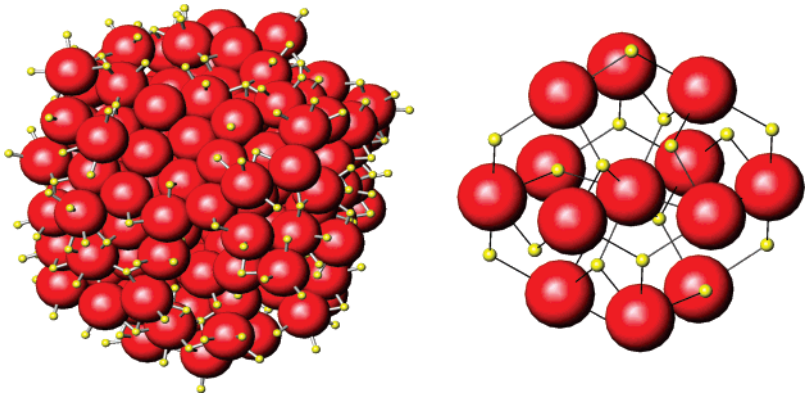

Figure 8. RMC generated 2 nm Ru (large circles in red) particle with sulfur atoms (small circles in yellow) on its surface (left). A fragment of RuS_2 crystal is shown on the right.

between the model atomic configuration and the simulation box, thus mimicking the finite particle size. To take into account the presence of undercoordinated Ru atoms at the free nanoparticle surface, only a fraction (50−75%) of Ru atoms in the model configurations was required to have 12 first neighbors. The presence of capping molecules (acetate/thiol) was not taken into account since only Ru−Ru correlations were seen in the experimental PDF data (see Figure 5). The RMC simulations for 4 nm Ru particles converged relatively fast as well and produced the model configurations shown in Figure 3 (lower part). The corresponding model PDFs and bond angle distributions are shown in Figures 6 and 7, respectively. The bond angle distribution in both sets of 4 nm Ru particles is broader than that in bulk Ru, reflecting the presence of a nonnegligible static atomic disorder in the former. That disorder is stronger in the thiol-capped particles since the two body (reflected by the PDF peaks) and three body (bond angles) atomic correlations appear to be weaker by approximately 15−20%, as measured by the ratio of the widths of the corresponding distributions, when compared to those in the particles not treated with dodecanethiol. Obviously, the degree of structural perfection in nanosized particles and, hence, their properties may be fine-tuned by post-preparation treatment and/or using suitable capping agents.

The model for the 2 nm thiol-capped Ru nanoparticle consisted of 188 ruthenium atoms forming a cluster (approximately 2 nm in size) positioned at the center of a simulation box with an edge of 20.5 Å. Sulfur atoms, 250 in total, were introduced sequentially close to the free surface of the Ru cluster until the PDF peak at approximately 2.3 Å was well-reproduced. Distances of minimal closest approach of 2.6, 2.28, and 2.05 Å for Ru−Ru, Ru−S, and S−S atoms, respectively, were imposed. Since 2 nm Ru particles exhibit a very high degree of structural distortion, no Ru−Ru coordination constraint was imposed; instead, the experimental PDF data were left to guide the spatial arrangement of Ru atoms in the model. Simulations were run with only Ru or S or both types of atoms moving around, turning on and off some of the constraints, until all important details in the experimental PDF data were well-reproduced as can be seen in Figure 6. The resulting model atomic configuration, which turned out to be a rather compact structure, is shown in Figure 8. The corresponding Ru−Ru−Ru bond angle distribution is shown in Figure 7. The rather smeared experimental PDF and Ru−Ru−Ru bond angle distributions of thiol-capped 2 nm Ru particles do not exhibit many of the characteristic features of the hcp-type structure of bulk Ru. Rather, they appear to be quite similar to those found with metallic glasses, suggesting that 2 nm Ru particles may well be viewed as an almost random close packing of atoms incorporating a core of Ru atoms covered by a Ru−S skin. Interestingly, sulfur and ruthenium atoms from that skin are arranged in a pattern similar to that observed in crystalline RuS_2[29] as the inspection of Figure 8 shows. No such requirement has been enforced in the model simulations.

Conclusion

High-energy XRD and atomic PDF analyses provide accurate structure data for nanosized materials, including catalysts, since the approach takes into account all components of the diffraction data, including Bragg-like and diffuse scattering, over an extended range of wave vectors. The data alone allow discrimination between competing structure models (e.g., hcp vs fcc) and may serve as a firm basis for 3-D computer simulations. Moreover, the approach/data is sensitive enough to reveal and quantify the presence of local structural distortions and even a core/shell-type nanoparticle sub-structure when they occur. Note that the presence of a protective skin/shell may greatly affect the catalytic activity/selectivity of nanosized particles. In particular, our studies find that both sets of 4 nm particles studied exhibit local structural distortions but yet may be described in terms of a periodic (hcp-type) model, involving a small number of parameters (local symmetry, unit cell, and atoms within it). When a more accurate structural description is needed, a nonperiodic atomic configuration, generated by RMC simulations, for example, that reflects both the atomic order and the local deviations from it may/should be used. Thiol-capped ruthenium particles of a size of 2 nm exhibit a great deal of structural disorder and a skin of sulfur atoms. A noncrystallographic model is the only accurate way to describe their atomic-scale structure. Noncrystallographic models involve a greater number of parameters (coordinates and types of all atoms in the model atomic configuration) than the crystallographic/periodic-type ones but, given the current advancement of computer power, can be used to compute, understand, and predict properties of nanosized particles/catalysts as well.

Acknowledgment. N.B. thanks Guillaume Evrard for help in using the RMC++ code and Milen Gateshki for help and insight in atomic PDF analysis. C.D. and G.V. acknowledge the French Ministry of Education and Research for financial support (ACI Nanoscience). This work was also supported by the NSF through Grant DMR 0304391(NIRT) and by CMU through Grant REF C602281. Use of the Advanced Photon Source was supported by the U.S. Department of Energy, Office of Basic Energy Sciences, under Contract DE-AC02-06CH11357.

References and Notes

(1) Zhang, H. et al. *Nature (London, U.K.)* **2003**, *424*, 1025.

(2) Crespo, P.; Litran, R.; Rojas, T. C.; Multinger, R.; del la Fluente, J. M.; Sanchez-Lopez, J. C.; Garcia, M. A.; Hernando, A.; Penades, S.; Fernandes, A. *Phys. Rev. Lett.* **2004**, *93*, 87204.

(3) Egami, T.; Billinge, S. J. L. *Underneath the Bragg Peaks*; Pergamon Press: Oxford, 2003.
(4) Petkov, V.; Zavalij, P. Y.; Lutta, S.; Whittingham, M. S.; Parvanov, V.; Shastri, S. *Phys. Rev. B: Condens. Matter Mater. Phys.* **2004**, *69*, 85410.
(5) Petkov, V.; Gateshki, M.; Niederberger, M.; Ren, Y. *Chem. Mater*. **2006**, *18*, 814.
(6) Petkov, V.; Parvanov, V.; Tomalia, D.; Swanson, D.; Bergstrom, D.; Vogt, T. *Solid State Commun.* **2005**, *134*, 671.
(7) Petkov, V.; Peng, Y.; Williams, G.; Huang, B.; Tomalia D.; Ren, Y. *Phys. Rev. B: Condens. Matter Mater. Phys.* **2005**, *72*, 195402.
(8) Geng, J. J. *Chem. Commun*. **2002**, 1112.
(9) Balint, I.; Miyazaki, A.; Aika, K. *J. Catal*. **2002**, *207*, 66.
(10) Zhang, Z.; Jackson, J. E.; Miller, D. *J. Appl. Catal., A: Gen.* **2001**, *219*, 89.
(11) Yang, J.; Lee, J. Y.; Deivaraz, T. C.; Too, H.-P. *J. Colloid Interface Sci*. **2004**, *271*, 308.
(12) Gao, S.; Zhang, J.; Zhu, Y.-F.; Che, C.-M. *New. J. Chem*. **2000**, *24*, 739.
(13)) Bonet, F.; Delmas, V.; Grugeon, S.; Urbina, R. H.; Silvert, P.-Y.; Tekaia-Elhsissen, K. *Nanostruct. Mater*. **1999**, *11*, 1277.
(14) Pan, C.; Pelzer, K.; Philipot, K.; Chaudret, B.; Dassenoy, F.; Lecante, P.; Casanove, M.-J. *J. Am. Chem. Soc*. **2001**, *123*, 7584.
(15) Vidoni, O.; Philipot, K.; Amiens, C.; Chaudret, B.; Balmes, O.; Malm, J.-O.; Bovin, J.-O.; Senocq, M.-J. *Angew. Chem., Int. Ed*. **1999**, *38*, 3736.
(16) Pelzer, K.; Vidoni, O.; Philipot, K.; Chaudret, B.; Colliere, V. *Adv. Funct. Mater*. **2003**, *15*, 118.
(17) Viau, G.; Brayner, R.; Poul, L.; Chakroune, N.; Lacaze, E.; Fievet-Vincent, F.; Fievet, F. *Chem. Mater*. **2003**, *15*, 486.
(18) Chakroune, N.; Viau, G.; Ammar, S.; Poul, L.; Veautier, D.; Chehimi, M. M.; Mangeney, C.; Villain, F.; Fievet, F. *Langmuir* **2005**, *21*, 6788.
(19) Klug, H. P.; Alexander, L. E. *X-ray Diffraction Procedures for Polycrystalline and Amorphous Materials*; John Wiley and Sons: New York, 1974.
(20) Swanson, H. E.; Fuyat, R. K.; Ugrinic, G. M. *Natl. Bureau Stand. Circ. (U.S.)* **1955**, *359*, 1.
(21) Petkov, V. *J. Appl. Crystallogr*. **1989**, *22*, 387.
(22) Proffen, T.; Billinge, S. J. L. *J. Appl. Crystallogr*. **1999**, *32*, 572.
(23) Ergun, S.; Schehl, S. R. *Carbon* **1973**, *11*, 127.
(24) Petkov, V.; Ohta, T.; Hou, Y.; Ren, Y. *J. Phys. Chem. C* **2007**, *111*, 714.
(25) Keen, D. A.; McGreevy, R. L. *Nature (London, U.K.)* **1990**, *344*, 423.
(26) Pusztai, L.; McGreevy, R. L. *Phys. Chem. Liq.* **1991**, *24*, 119.
(27) Howe, M. A.; McGreevy, R. L.; Pusztai, L.; Borzsak, I. *Phys. Chem. Liq.* **1993**, *25*, 204.
(28) Evrard, G.; Pusztai, L. *J. Phys.: Condens. Matter* **2005**, *17*, 1.
(29) Zeng, Y.; Holzman, N. A. W. *Phys. Rev. B: Condens. Matter Mater. Phys.* **1994**, *50*, 8214.